Journal of Nuclear Materials 596 (2024) 155104

Contents lists available at ScienceDirect

Journal of Nuclear Materials

journal homepage: www.elsevier.com/locate/jnucmat

Short communication

Deformation localisation in ion-irradiated Fe and Fe10Cr

Kay Song [a,*], Dina Sheyfer [b], Wenjun Liu [b], Jonathan Z. Tischler [b], Suchandrima Das [c], Kenichiro Mizohata [d], Hongbing Yu [f], David E.J. Armstrong [e], Felix Hofmann [a]

[a] Department of Engineering Science, University of Oxford, Parks Road, Oxford, OX1 3PJ, UK
[b] X-ray Science Division, Argonne National Laboratory, 9700 South Cass Avenue, Lemon, IL 60439, USA
[c] Department of Mechanical Engineering, University of Bristol, Queen's Building, University Walk, Bristol, BS8 1TR, UK
[d] Department of Physics, University of Helsinki, P.O. Box 43, 00014 Helsinki, Finland
[e] Department of Materials, University of Oxford, Parks Road, Oxford, OX1 3PH, UK
[f] Canadian Nuclear Laboratories, Chalk River, ON K0J 1J0, Canada

GRAPHICAL ABSTRACT

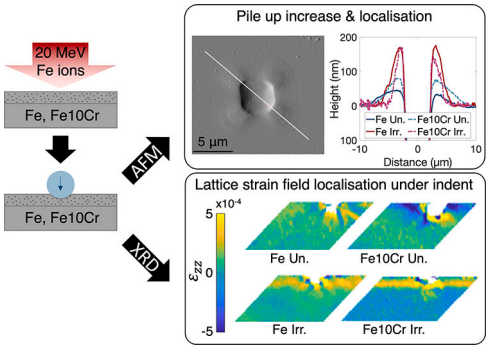

ARTICLE INFO

Dataset link: https://doi.org/10.5281/zenodo.11059510

Keywords:
Ferritic steels
Ion-irradiation
Plastic deformation
Atomic force microscopy
Synchrotron radiation

ABSTRACT

Determining the mechanisms for irradiation-induced ductility loss is crucial for the design of reactor structural components. Here, the deformation characteristics around nanoindents in Fe and Fe10Cr irradiated with Fe ions to ~1 displacement-per-atom at 313 K are non-destructively studied. Slip steps surrounding the nanoindents indicate that deformation is localised in the irradiated materials. Lattice rotation and strain fields near the indent site show over 87% confinement of plasticity in the irradiated material. Cr has little effect on the irradiation-induced changes in pile-up topography and deformation fields, suggesting it has limited impact on retaining strain hardening capacity and reducing irradiation-induced embrittlement.

1. Main text

Understanding the mechanical behaviour of structural materials is essential for the design and operation of next-generation nuclear reactors. Reduced-activation ferritic/martensitic steels are promising candidates due to their good thermomechanical properties and resistance to irradiation swelling [1]. Nevertheless, neutron irradiation in reactor environments will still lead to increased hardening and reduced ductility

* Corresponding author.
E-mail addresses: kay.song@eng.ox.ac.uk (K. Song), felix.hofmann@eng.ox.ac.uk (F. Hofmann).

https://doi.org/10.1016/j.jnucmat.2024.155104
Received 21 February 2024; Received in revised form 9 April 2024; Accepted 15 April 2024
Available online 23 April 2024

Table 1
Manufacturer-provided chemical compositions as measured by glow discharge mass spectrometry [36,37].

Alloy	Cr (wt%)	C (wppm)	S (wppm)	O (wppm)	N (wppm)	Grain Size (μm)
Fe	<0.0002	4	2	4	1	187 ± 150
Fe10Cr	10.10	4	4	4	3	98 ± 55

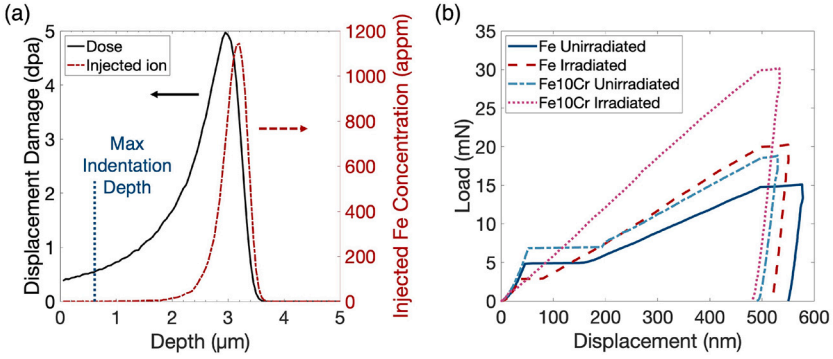

Fig. 1. (a) The irradiation damage and injected ion profiles as calculated by SRIM [38]. (b) Representative load-displacement curves from each material.

of structural steels [2,3]. Studies into the effect of microstructure and composition to mitigate these irradiation-induced changes are crucial [4–6].

A well-known phenomenon following the deformation of irradiated materials is deformation localisation [7–12]. Here, localisation refers to deformation occurring preferentially in certain regions of the material, such as channels. The accepted mechanism is that glide dislocations annihilate irradiation-induced defects [13,14]. This creates easy glide channels with a locally reduced density of irradiation-induced defects that confine subsequent deformation [15]. The formation of these channels contributes to irradiation embrittlement and irradiation-assisted stress corrosion cracking [16].

Presently, the exact details of the mechanisms by which irradiation defects are removed still remain unclear. This is an active area for modelling and simulations [17–19]. However, there is a lack of experimental investigations to validate modelling predictions. Transmission electron microscopy (TEM) is a common way to directly observe dislocation microstructures and channels [20–22]. However, TEM is unable to provide information, especially in 3D, on the local stress and strain states, which are key to compare with simulations. A non-destructive method such as X-ray diffraction can uniquely provide information over a greater volume and in 3D [23,24].

Here, we consider the deformation microstructure around nanoindents in Fe and Fe with 10% Cr by weight, hereafter referred to as Fe10Cr, for both the unirradiated material and following irradiation with Fe ions at 313 K. This allows the study of the effect of irradiation and Cr content. Surface topography around the indent site was examined with atomic force microscopy (AFM). 3D lattice rotation and strain fields under the surface were probed by X-ray Laue diffraction. The samples used in this study are the same as those in previous studies of irradiation-induced lattice strain, thermal and mechanical properties [25–27]. The materials from which the samples are taken have also been investigated extensively in other irradiation studies [28–34]. This is important, as it helps to build a comprehensive understanding of the different aspects of irradiation damage whilst maintaining consistent sample processing and irradiation history [35].

The Fe and Fe10Cr materials were manufactured under the European Fusion Development Agreement (EFDA) programme (contract EFDA-06-1901) and their chemical composition is listed in Table 1. The materials were made by induction melting under an argon atmosphere followed by cold-forging and heat treatments [36,37].

The samples were mechanically ground with SiC paper, and then polished with diamond suspension and colloidal silica (0.04 μm). Finally, they were electropolished to achieve a deformation-free surface finish.

Ion irradiation was performed with 20 MeV Fe^{4+} ions using the tandem accelerator at the University of Helsinki. The samples were actively held at 313 K during irradiation. The dose profile shown in Fig. 1(a) was calculated with SRIM (Stopping and Range of Ion in Matter) using the Quick K-P model [38] with 20 MeV Fe ions on a Fe target with 40 eV displacement energy [39] at normal incidence. The calculated damaged layer extends to 3.5 μm below the sample surface. The average dose in the top 580 nm, which is the maximum indentation depth (including creep), is 0.46 displacements-per-atom (dpa). The damage profile peaks at 5 dpa at a depth of 3 μm. The average dose of the whole damage layer is 1.7 dpa.

Consistent grain orientation across different samples is important as the pile-up morphology is expected to show orientation dependence from previous studies of body-centred cubic (BCC) materials [40,41]. Those studies also found that pile-up heights are the most sensitive to irradiation-induced changes when indenting along the ⟨001⟩ direction. In this study, electron backscatter diffraction was used to identify grains within 5° of ⟨001⟩ out-of-plane orientation on each sample for investigation with AFM and X-ray Laue diffraction. Further information about the grain orientations can be found in the Supplementary File.

Nanoindentation was performed using an MTS Nano Indenter XP with a spherical diamond tip of 5 μm nominal radius (Synton-MDP). Load-controlled indentation was performed to a nominal depth of 500 nm, with a hold segment of 10 s before unloading. The indentation depth was chosen to be less than 20% of the damaged layer thickness to ensure that a majority of the plastic zone is contained in the irradiated layer [42,43].

The load-displacement curves (Fig. 1(b)) for all materials show similar initial Hertzian elastic contact segments. Pop-in events occurred in all samples, and the irradiated samples show lower pop-in loads than the unirradiated samples possibly due to irradiation defects acting as extra sources of dislocation nucleation [26,44,45].

Analysis of the peak loads of at least 6 indents on each sample was performed to obtain an indication of the material hardness. Large pop-in loads were often observed for the unirradiated materials due to low populations of pre-existing dislocations. As a result, many indentation tests on the pre-identified grains exceed 500 nm in depth, and could not be used.

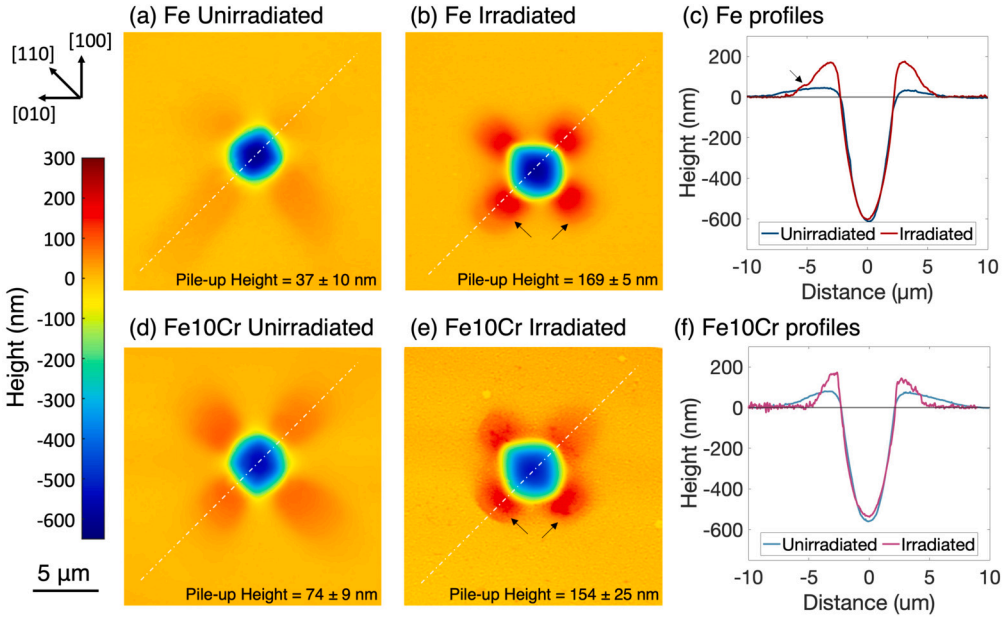

Fig. 2. The pile-up topography surrounding the indent site for (a) unirradiated Fe and (b) irradiated Fe. The average pile-up heights are calculated from repeated measurements of the 4 pile-up lobes surrounding each indent, with the associated standard deviations shown. The white dashed line indicates the profile of pile-up height taken from the measurements and shown in (c). The same layout for Fe10Cr is shown in (d)–(f). Black arrows indicate evidence of slip steps (further details in the Supplementary File). (For interpretation of the colours in the figure, the reader is referred to the web version of this article.)

Solid solution hardening in the unirradiated materials is observed from a 20% (±6%) increase in peak load between Fe and Fe10Cr. Irradiation resulted in a 21% (±8%) increase in peak load for Fe and a 43% (±7%) increase for Fe10Cr. This agrees with hardness trends from previous measurements with Berkovich nanoindentation, which show a 31% (±5%) increase for Fe and a 48% (±7%) increase for Fe10Cr following irradiation [27]. The creep distance from holding the peak load is greater in Fe than Fe10Cr for both the unirradiated and irradiated materials.

Pile-up topography around the indent sites (Fig. 2) was measured with a Veeco MultiMode 8 atomic force microscope (AFM) in ScanAsyst^{TM} mode. There is a four-fold symmetry in the pile-up pattern due to the indents being made on grains with close to ⟨001⟩ out-of-plane orientation. The pile-up lobes are oriented along the ⟨110⟩ directions, which has been previously observed in other BCC materials [40,41,46,47].

For the unirradiated samples, the pile-up height increases with the addition of Cr from 37 ± 10 nm for Fe to 74 ± 9 nm for Fe10Cr. Pile-up has been found to increase with decreasing strain hardening exponents [48–50]. This suggests that the presence of Cr reduces strain hardening capacity. Indeed, this is consistent with our previous study of the same materials [26], which shows from nanoindentation stress-strain curves that strain hardening capacity decreases with Cr content in unirradiated FeCr.

Pile-up height increases after irradiation for Fe and Fe10Cr to 169 ± 5 nm and 154 ± 25 nm, respectively. The increase in average pile-up height is consistent with previous findings of irradiation-induced strain hardening capacity reduction [26,51,52]. The presence of Cr has little effect on the pile-up height following irradiation. This is consistent with previous findings from stress-strain studies of the same materials, where strain hardening exponents were reduced to zero regardless of Cr content, even for a dose that is 90% lower than the current study [26]. Hardie et al. [53] also observed an increase in pile-up height for Fe12Cr following irradiation to 6.18 dpa. However, the orientation of the grains was not specified, which is known to significantly affect pile-up behaviour [40,41,54].

The pile-up topography is more spatially confined in the irradiated samples, only extending to ± 5 μm on either side of the indent centre along the ⟨110⟩ direction (Fig. 2(c) and (f)). In contrast, the lobes of the unirradiated materials extend up to 10 μm away from the indent. Slip steps are also observed in the pile-up of the irradiated material (black arrows in Fig. 2(b), (c), and (e)). Hardie et al. [55] previously found that slip steps on the surface of ion-irradiated Fe12Cr result from shear bands beneath the surface, associated with defect-free channels in the irradiated layer. These channels lead to irradiation-induced strain softening and localisation of deformation [56].

Lattice rotation and strains around the nanoindents were measured with micro-beam X-ray Laue diffraction at the 34-ID-E beamline at the Advanced Photon Source (Argonne National Laboratory, IL, USA). Differential Aperture X-ray Microscopy (DAXM) was used to obtain depth resolution into the surface of the material. The technique has been described in detail elsewhere [57–59]. Here, the sample was mounted in a 45° reflection geometry. The polychromatic incident beam (7–30 keV) is focused on the sample surface with a size of 170×240 nm^2. For each sample, a $30 \times 40 \times 20$ μm^3 volume was probed with $1.1 \times 1.5 \times 1$ μm^3 3D spatial resolution. Due to the sample mounting geometry, the path of the beam was at 45° to the sample surface. Hence the edges of the volume probed by X-rays are also confined by that angle (Fig. 3 and 4). Further details of the set-up are included in the Supplementary File.

The orientation distribution and strain refinement calculations [60] were performed using LaueGo [61]. The calculation of lattice rotation from the orientation of each voxel, data interpolation, and visualisation of the lattice rotation and strain field were performed with code modified from [12,23]. The reference lattice orientation was calculated from the average orientation between 18–20 μm below the sample surface.

The lattice rotations in the unirradiated Fe extend to over 20 μm away from the indentation site (Fig. 3(a)). There is a long 'streak' present in the θ_x map, similar to previous measurements in tungsten [23,46]. The rotation fields of Fe10Cr (Fig. 3(c)) are similar in spatial extent and distribution to Fe.

The extent of the rotation field induced by indentation in the irradiated samples is more confined than in the unirradiated material. This is particularly noticeable for the Fe sample (Fig. 3(b)), where the rotation field is predominantly the top 5 μm in the z-direction, and ~7 μm in the x- and y-directions. The distribution of lattice rotations in the irradiated Fe10Cr sample (Fig. 3(d)) is similar to the irradiated Fe, with some ex-

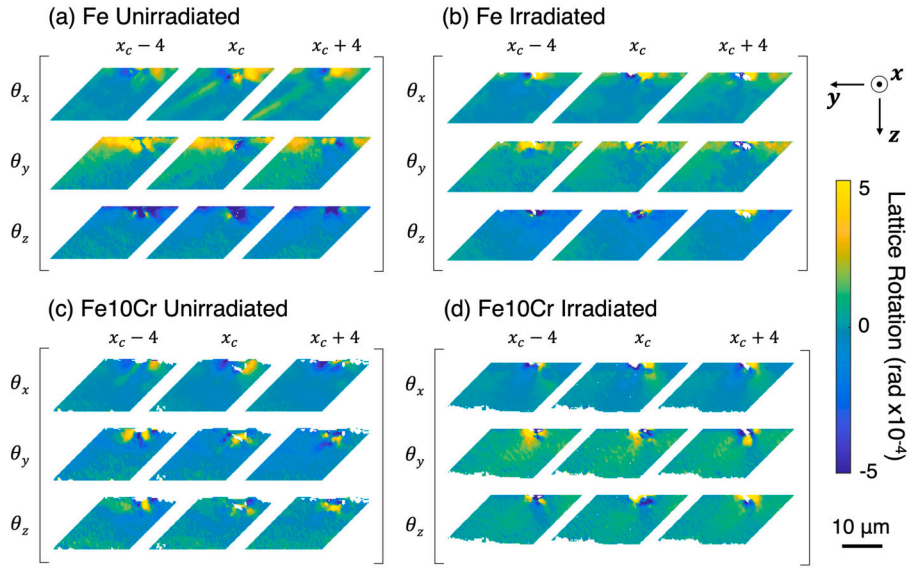

Fig. 3. The lattice rotation under the indent for the different samples in this study. The $\boldsymbol{x} - \boldsymbol{y}$ plane is parallel to the surface of the bulk sample, while $\boldsymbol{z}$ points into the bulk material. For each sample, the lattice rotations components (θ_x, θ_y, and θ_z) are presented from 3 slices (parallel to the $\boldsymbol{y} - \boldsymbol{z}$ plane). The middle slice ($x = x_c$) is taken through the centre of the indent. The slices on either side are at a distance of 4 µm from the centre in the $\boldsymbol{x}$-direction. Magnified plots of each sample are included in the Supplementary File. (For interpretation of the colours in the figure, the reader is referred to the web version of this article.)

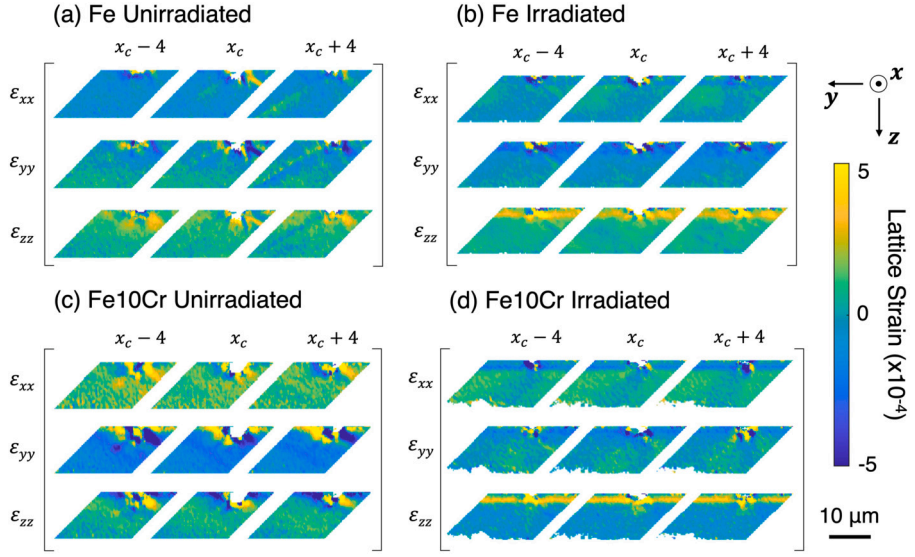

Fig. 4. The 3 principal components of the deviatoric strain tensor, ϵ_{xx}, ϵ_{yy}, and ϵ_{zz} in the samples. The orientation of the measurements and the slicing convention are the same as described in Fig. 3. Magnified plots of each sample are included in the Supplementary File. (For interpretation of the colours in the figure, the reader is referred to the web version of this article.)

tended regions of smaller lattice rotations ($|\theta| < 3 \times 10^{-4}$ radians) up to 10 µm from the indent centre. This represents a reduction of over 87% of the volume containing lattice rotations. This is the same ratio as determined by the lateral extent of pile-up from AFM measurements, even though the absolute radius of the deformed volume measured by X-ray diffraction is twice as large. The volume over which the deformation zone is defined is illustrated in the Supplementary File.

The spatial distribution of tensile (positive) and compressive (negative) strain is similar between the unirradiated samples of Fe and Fe10Cr (Fig. 4). However, the spatial extent and magnitude of strain, both tensile and compressive, are greater in Fe10Cr than in Fe. This could be attributed to the greater peak load applied to Fe10Cr to reach the same indentation depth as in Fe (Fig. 1(b)), due to its higher yield strength, which in turn leads to greater residual stresses.

After irradiation, there is a large tensile strain in the $\boldsymbol{z}$ direction for Fe and Fe10Cr at a depth of ~3 µm (Fig. 4(b) and (d)). This is likely due to the presence of injected Fe ions from irradiation, as previously observed [25,27]. There is a corresponding compressive strain of lower magnitude in the $\boldsymbol{x}$- and $\boldsymbol{y}$-directions. Furthermore, the magnitudes of ϵ_{xx} and ϵ_{yy} are similar, which is consistent with irradiation-induced lattice swelling and the presence of the external boundary condition requiring geometric continuity between the irradiated layer and the unirradiated bulk [59].

For both the irradiated Fe and Fe10Cr materials, the spatial extent of the strain field beneath and surrounding the indent is predominantly present in the top 3–4 µm along the $\boldsymbol{z}$-direction (Fig. 4(b) and (d)). The confinement of the strain field is largely within the irradiated layer, with rapidly vanishing strains at depths beyond that. Similar to lattice rotation fields, the extent of the strain fields in the $\boldsymbol{x}$- and $\boldsymbol{y}$-directions is also reduced following irradiation for both Fe and Fe10Cr. The 'high strain' zone volume is illustrated in the Supplementary File. It appears that the presence of 10% Cr content does not significantly affect the

strain states following irradiation and deformation. This is despite a ~50% increase in applied load for the irradiated Fe10Cr material to achieve the same indentation depth as the irradiated Fe sample.

The confinement of lattice rotation and strain fields in the irradiated Fe and Fe10Cr is consistent with previous observations of plastic zone confinement in irradiated Fe12Cr [53,55]. From TEM lift-outs taken through indent cross-sections, it was observed that the spatial extent of dislocation propagation reduced by 24–31% in the irradiated material.

Combining the nanoindentation, AFM, and DAXM measurements, we can formulate a comprehensive picture of plasticity in ion-irradiated Fe and Fe10Cr. Without irradiation, the presence of Cr causes solid solution hardening. This necessitates a greater indentation load for Fe10Cr than Fe to reach the same indentation depth. As such, the residual strains are greater. Furthermore, the presence of Cr also reduces the strain hardening capacity of the material, which leads to a greater pile-up height in Fe10Cr.

Ion irradiation introduces defects in the material that act as obstacles to glide dislocations, causing hardening. Even though the inclusion of 10%Cr causes a similar amount of net hardening as introducing irradiation defects in Fe, the respective pile-up topography and residual lattice rotation and strain fields are very different. The great increase in pile-up height due to irradiation (~450% for Fe) reflects a dramatic reduction in strain hardening capacity, as previously observed from nanoindentation stress-strain curves of the same materials [26]. In comparison, the pile-up height only increases ~200% from the addition of 10%Cr to Fe in the unirradiated case, despite showing similar hardening. The mechanism of strain softening in the irradiated material can be explained by the observation of slip steps, an indication of dislocation channelling, which provides paths for subsequently-generated glide dislocations to move at a lower stress. This causes slip localisation where deformation preferentially occurs in the dislocation channels. Irradiation-induced strain softening also causes a corresponding confinement in the lateral extent of pile-up topography. We directly observed plastic zone confinement of over 87% in the irradiated materials from the localisation of lattice strain and rotation fields surrounding the indents.

The effect of Cr on the post-irradiation deformation behaviour is limited. Even though the irradiation-induced hardening is much greater in Fe10Cr than in Fe, the height and spatial extent of the pile-up topography are very similar for both irradiated materials. This supports previous observations that post-irradiation reduction in strain hardening capacity does not depend on Cr [26]. In this study, we also observed the effect of this on the lattice rotation and strain fields in both Fe and Fe10Cr, which were reduced to similar extents following irradiation. The 3D measurements in this study also provide valuable comparisons for future modelling studies, which will be crucial to understanding the mechanical properties of reactor structural materials in operation.

In summary, deformation localisation has been characterised in ion-irradiated Fe and Fe10Cr following nanoindentation. Following irradiation, there is an increase in pile-up height, spatial confinement of the pile-up topography, and formation of slip steps, indicating slip localisation. Lattice rotation and strain fields surrounding the indent in the irradiated material are confined to a volume less than 13% of that in the unirradiated materials. In practice, the localisation of deformation and the confinement of plastic zones means that a material is less able to absorb energy associated with deformation, leading to embrittlement. Despite significant differences in irradiation hardening, the irradiated Fe and Fe10Cr materials show very similar pile-up topography and deformation fields. Our results suggest that Cr content does not seem to mitigate the loss of strain hardening capacity. This means that strategies other than varying the composition of steels are required to retain post-irradiation ductility, a key consideration to guide the design of future reactor component materials.

Funding

This research used resources of the Advanced Photon Source, a U.S. Department of Energy (DOE) Office of Science User Facility operated for the DOE Office of Science by Argonne National Laboratory under Contract No. DE-AC02-06CH11357. The study was also supported by Laboratory Direct Research and Development (LDRD) funding from Argonne National Laboratory, provided by the Office of Science (OS), of the U.S. Department of Energy (DOE) under the same contract. The authors acknowledge use of characterisation facilities within the David Cockayne Centre for Electron Microscopy, Department of Materials, University of Oxford, alongside financial support provided by the Henry Royce Institute (grant EP/R010145/1). KS acknowledges funding from the General Sir John Monash Foundation and the University of Oxford Department of Engineering Science. FH acknowledges funding from the European Research Council (ERC) under the European Union's Horizon 2020 research and innovation programme (grant 714697). DEJA acknowledges funding from EPSRC (grant EP/P001645/1).

CRediT authorship contribution statement

Kay Song: Writing – review & editing, Writing – original draft, Visualization, Software, Methodology, Investigation, Formal analysis. **Dina Sheyfer:** Writing – review & editing, Investigation. **Wenjun Liu:** Writing – review & editing, Investigation. **Jonathan Z. Tischler:** Writing – review & editing, Software, Investigation. **Suchandrima Das:** Visualization, Software. **Kenichiro Mizohata:** Resources. **Hongbing Yu:** Writing – review & editing, Resources. **David E.J. Armstrong:** Writing – review & editing, Supervision. **Felix Hofmann:** Writing – review & editing, Supervision, Resources, Conceptualization.

Declaration of competing interest

The authors declare that they have no known competing financial interests or personal relationships that could have appeared to influence the work reported in this paper.

Data and code availability

All data, raw and processed, as well as the processing and plotting scripts are available at: https://doi.org/10.5281/zenodo.11059510

Acknowledgements

The authors are grateful to R J Scales (Department of Materials, University of Oxford) for their help with AFM training.

Appendix A. Supplementary material

Supplementary material related to this article can be found online at https://doi.org/10.1016/j.jnucmat.2024.155104.

References

[1] N. Baluc, R. Schäublin, P. Spätig, M. Victoria, On the potentiality of using ferritic/martensitic steels as structural materials for fusion reactors, Nucl. Fusion 44 (1) (2004) 56–61, https://doi.org/10.1088/0029-5515/44/1/006.

[2] R.J. Kurtz, G.R. Odette, Overview of reactor systems and operational environments for structural materials in fusion reactors, Struct. Alloy. Nucl. Energy Appl. (2019) 51–102, https://doi.org/10.1016/B978-0-12-397046-6.00003-4.

[3] S.J. Zinkle, Fusion materials science: overview of challenges and recent progress, Phys. Plasmas 12 (5) (2005) 058101, https://doi.org/10.1063/1.1880013.

[4] A. Bhattacharya, X. Chen, T. Graening, J.W. Geringer, J. Reed, J. Henry, L. Pilloni, D. Terentyev, A. Puype, T.S. Byun, Y. Katoh, M. Rieth, S.J. Zinkle, Irradiation hardening and ductility loss of Eurofer97 steel variants after neutron irradiation to ITER-TBM relevant conditions, Fusion Eng. Des. 173 (112) (2021) 935, https://doi.org/10.1016/j.fusengdes.2021.112935.

[5] M. Rieth, E. Simondon, G. Pintsuk, G. Aiello, J. Henry, D. Terentyev, A. Puype, C. Cristalli, L. Pilloni, O. Tassa, M. Klimenkov, H.-C. Schneider, P. Fernandez, T. Gräning, X. Chen, A. Bhattacharya, J. Reed, J. Geringer, M. Sokolov, Y. Katoh, L. Snead, Technological aspects in blanket design: effects of micro-alloying and thermo-mechanical treatments of EUROFER97 type steels after neutron irradiation, Fusion Eng. Des. 168 (112) (2021) 645, https://doi.org/10.1016/j.fusengdes.2021.112645.
[6] S. Oh, J. Lee, C. Jang, A. Kimura, Irradiation hardening and embrittlement in high-Cr oxide dispersion strengthened steels, J. Nucl. Mater. 386–388 (2009) 503–506, https://doi.org/10.1016/j.jnucmat.2008.12.144.
[7] J.V. Sharp, Deformation of neutron-irradiated copper single crystals, Philos. Mag. 16 (139) (1967) 77–96, https://doi.org/10.1080/14786436708229258.
[8] K. Farrell, T. Byun, N. Hashimoto, Deformation mode maps for tensile deformation of neutron-irradiated structural alloys, J. Nucl. Mater. 335 (3) (2004) 471–486, https://doi.org/10.1016/j.jnucmat.2004.08.006.
[9] N. Hashimoto, T.S. Byun, K. Farrell, S.J. Zinkle, Deformation microstructure of neutron-irradiated pure polycrystalline metals, J. Nucl. Mater. Part B 329–333 (1–3) (2004) 947–952, https://doi.org/10.1016/J.JNUCMAT.2004.04.063.
[10] T.S. Byun, N. Hashimoto, Strain localization in irradiated materials, Nucl. Eng. Des. 38 (7) (2006) 619–638.
[11] S. Zinkle, Radiation-Induced Effects on Microstructure, Compr. Nucl. Mater., vol. 1, Elsevier, 2012, pp. 65–98.
[12] S. Das, H. Yu, E. Tarleton, F. Hofmann, Hardening and strain localisation in helium-ion-implanted tungsten, Sci. Rep. 9 (1) (2019) 18354, https://doi.org/10.1038/s41598-019-54753-3.
[13] G. Saada, J. Washburn, Interaction between prismatic and glissile dislocations, Tech. Rep., Lawrence Livermore National Laboratory (LLNL), Livermore, CA (United States), 1962.
[14] A.J.E. Foreman, J.V. Sharp, A mechanism for the sweeping-up of loops by glide dislocations during deformation, Philos. Mag. 19 (161) (1969) 931–937, https://doi.org/10.1080/14786436908225858.
[15] E.A. Little, Neutron-irradiation hardening in irons and ferritic steels, Int. Met. Rev. 21 (1) (1976) 25–60, https://doi.org/10.1179/IMTR.1976.21.1.25.
[16] S. Zinkle, G. Was, Materials challenges in nuclear energy, Acta Mater. 61 (3) (2013) 735–758, https://doi.org/10.1016/j.actamat.2012.11.004.
[17] A. Patra, D.L. McDowell, Continuum modeling of localized deformation in irradiated bcc materials, J. Nucl. Mater. 432 (1–3) (2013) 414–427, https://doi.org/10.1016/j.jnucmat.2012.08.021.
[18] A. Patra, D.L. McDowell, Crystal plasticity investigation of the microstructural factors influencing dislocation channeling in a model irradiated bcc material, Acta Mater. 110 (2016) 364–376, https://doi.org/10.1016/j.actamat.2016.03.041.
[19] Y. Cui, N. Ghoniem, G. Po, Plasticity of irradiated materials at the nano and micro-scales, J. Nucl. Mater. 546 (152) (2021) 746, https://doi.org/10.1016/j.jnucmat.2020.152746.
[20] S. Zinkle, B. Singh, Microstructure of neutron-irradiated iron before and after tensile deformation, J. Nucl. Mater. 351 (1–3) (2006) 269–284, https://doi.org/10.1016/j.jnucmat.2006.02.031.
[21] M.N. Gussev, K.G. Field, J.T. Busby, Deformation localization and dislocation channel dynamics in neutron-irradiated austenitic stainless steels, J. Nucl. Mater. 460 (2015) 139–152, https://doi.org/10.1016/j.jnucmat.2015.02.008.
[22] Y. Dai, X. Jia, J. Chen, W. Sommer, M. Victoria, G. Bauer, Microstructure of both as-irradiated and deformed 304L stainless steel irradiated with 800 MeV protons, J. Nucl. Mater. 296 (1–3) (2001) 174–182, https://doi.org/10.1016/S0022-3115(01)00565-7.
[23] S. Das, D. Armstrong, Y. Zayachuk, W. Liu, R. Xu, F. Hofmann, The effect of helium implantation on the deformation behaviour of tungsten: X-ray micro-diffraction and nanoindentation, Scr. Mater. 146 (2018) 335–339, https://doi.org/10.1016/j.scriptamat.2017.12.014.
[24] G. Altinkurt, M. Fèvre, G. Geandier, M. Dehmas, O. Robach, J.-S. Micha, Local strain redistribution in a coarse-grained nickel-based superalloy subjected to shot-peening, fatigue or thermal exposure investigated using synchrotron X-ray Laue microdiffraction, J. Mater. Sci. 53 (11) (2018) 8567–8589, https://doi.org/10.1007/s10853-018-2144-4.
[25] K. Song, S. Das, A. Reza, N.W. Phillips, R. Xu, H. Yu, K. Mizohata, D.E. Armstrong, F. Hofmann, Characterising ion-irradiated FeCr: hardness, thermal diffusivity and lattice strain, Acta Mater. 201 (2020) 535–546, https://doi.org/10.1016/j.actamat.2020.10.015.
[26] K. Song, H. Yu, P. Karamched, K. Mizohata, D.E.J. Armstrong, F. Hofmann, Deformation behaviour of ion-irradiated FeCr: a nanoindentation study, J. Mater. Res. 37 (12) (2022) 2045–2060, https://doi.org/10.1557/s43578-022-00613-2.
[27] K. Song, D. Sheyfer, K. Mizohata, M. Zhang, W. Liu, D. Gürsoy, D. Yang, I. Tolkachev, H. Yu, D.E. Armstrong, F. Hofmann, Dose and compositional dependence of irradiation-induced property change in fecr, J. Nucl. Mater. 594 (154) (2024) 998, https://doi.org/10.1016/j.jnucmat.2024.154998.
[28] R. Schäublin, B. Décamps, A. Prokhodtseva, J.F. Löffler, On the origin of the primary 1/2 a0 < 111 > and a0 < 100 > loops in irradiated Fe(Cr) alloys, Acta Mater. 133 (2017) 427–439, https://doi.org/10.1016/j.actamat.2017.02.041.
[29] C.D. Hardie, C.A. Williams, S. Xu, S.G. Roberts, Effects of irradiation temperature and dose rate on the mechanical properties of self-ion implanted Fe and Fe–Cr alloys, J. Nucl. Mater. 439 (1–3) (2013) 33–40, https://doi.org/10.1016/j.jnucmat.2013.03.052.
[30] A. Bhattacharya, E. Meslin, J. Henry, A. Barbu, S. Poissonnet, B. Décamps, Effect of chromium on void swelling in ion irradiated high purity Fe–Cr alloys, Acta Mater. 108 (2016) 241–251, https://doi.org/10.1016/j.actamat.2016.02.027.
[31] D. Brimbal, B. Décamps, J. Henry, E. Meslin, A. Barbu, Single- and dual-beam in situ irradiations of high-purity iron in a transmission electron microscope: effects of heavy ion irradiation and helium injection, Acta Mater. 64 (2014) 391–401, https://doi.org/10.1016/j.actamat.2013.10.052.
[32] D. Brimbal, E. Meslin, J. Henry, B. Décamps, A. Barbu, He and Cr effects on radiation damage formation in ion-irradiated pure iron and Fe–5.40 wt.% Cr: a transmission electron microscopy study, Acta Mater. 61 (13) (2013) 4757–4764, https://doi.org/10.1016/J.ACTAMAT.2013.04.070.
[33] M. Roldán, P. Fernández, R. Vila, A. Gómez-Herrero, F. Sánchez, The effect of triple ion beam irradiation on cavity formation on pure EFDA iron, J. Nucl. Mater. 479 (2016) 100–111, https://doi.org/10.1016/j.jnucmat.2016.06.043.
[34] Y.-R. Lin, A. Bhattacharya, D. Chen, J.-J. Kai, J. Henry, S.J. Zinkle, Temperature-dependent cavity swelling in dual-ion irradiated Fe and Fe-Cr ferritic alloys, Acta Mater. 207 (116) (2021) 660, https://doi.org/10.1016/j.actamat.2021.116660.
[35] X. Xiao, L. Yu, Nano-indentation of ion-irradiated nuclear structural materials: a review, Nucl. Mater. Energy 22 (2020) 100721, https://doi.org/10.1016/j.nme.2019.100721.
[36] J.L. Coze, Procurement of pure Fe metal and Fe-based alloys with controlled chemical alloying element contents and microstructure, Tech. Rep., ARMINES Ecole Nationale Superieure des Mines, 2007.
[37] A. Fraczkiewicz, Material Delivery Report BC4000483543/P5B51, Tech. Rep., Ecole des Mines, France, 2011.
[38] J.F. Ziegler, M.D. Ziegler, J.P. Biersack, SRIM - the stopping and range of ions in matter (2010), Nucl. Instrum. Methods Phys. Res., Sect. B, Beam Interact. Mater. Atoms 268 (11–12) (2010) 1818–1823, https://doi.org/10.1016/j.nimb.2010.02.091.
[39] ASTM E521, Standard Practice for Investigating the Effects of Neutron Radiation Damage Using Charged-Particle Irradiation, Annu. B. ASTM Stand., vol. 12.02, ASTM International, West Conshohocken, PA, 2016.
[40] S. Das, H. Yu, E. Tarleton, F. Hofmann, Orientation-dependent indentation response of helium-implanted tungsten, Appl. Phys. Lett. 114 (22) (2019) 221905, https://doi.org/10.1063/1.5097403.
[41] S. Das, H. Yu, K. Mizohata, E. Tarleton, F. Hofmann, Modified deformation behaviour of self-ion irradiated tungsten: a combined nano-indentation, HR-EBSD and crystal plasticity study, Int. J. Plast. 135 (2020) 102817, https://doi.org/10.1016/j.ijplas.2020.102817.
[42] M. Mata, O. Casals, J. Alcalá, The plastic zone size in indentation experiments: the analogy with the expansion of a spherical cavity, Int. J. Solids Struct. 43 (20) (2006) 5994–6013, https://doi.org/10.1016/j.ijsolstr.2005.07.002.
[43] J. Chen, S. Bull, On the relationship between plastic zone radius and maximum depth during nanoindentation, Surf. Coat. Technol. 201 (7) (2006) 4289–4293, https://doi.org/10.1016/j.surfcoat.2006.08.099.
[44] K. Jin, Y. Xia, M. Crespillo, H. Xue, Y. Zhang, Y.F. Gao, H. Bei, Quantifying early stage irradiation damage from nanoindentation pop-in tests, Scr. Mater. 157 (2018) 49–53, https://doi.org/10.1016/j.scriptamat.2018.07.035.
[45] S. Pathak, S.R. Kalidindi, J.S. Weaver, Y. Wang, R.P. Doerner, N.A. Mara, Probing nanoscale damage gradients in ion-irradiated metals using spherical nanoindentation, Sci. Rep. 7 (1) (2017) 1–12, https://doi.org/10.1038/s41598-017-12071-6.
[46] H. Yu, S. Das, H. Yu, P. Karamched, E. Tarleton, F. Hofmann, Orientation dependence of the nano-indentation behaviour of pure Tungsten, Scr. Mater. 189 (2020) 135–139, https://doi.org/10.1016/j.scriptamat.2020.08.014.
[47] R. Smith, D. Christopher, S.D. Kenny, A. Richter, B. Wolf, Defect generation and pileup of atoms during nanoindentation of Fe single crystals, Phys. Rev. B 67 (24) (2003) 245405, https://doi.org/10.1103/PhysRevB.67.245405.
[48] B. Taljat, G. Pharr, Development of pile-up during spherical indentation of elastic–plastic solids, Int. J. Solids Struct. 41 (14) (2004) 3891–3904, https://doi.org/10.1016/j.ijsolstr.2004.02.033.
[49] R. Hill, B. Storakers, A.B. Zdunek, A theoretical study of the Brinell hardness test, Proc. R. Soc. Lond. Ser. A, Math. Phys. Sci. 423 (1865) (1989) 301–330, https://doi.org/10.1098/rspa.1989.0056.
[50] S. Biwa, An analysis of fully plastic Brinell indentation, J. Mech. Phys. Solids 43 (8) (1995) 1303–1333, https://doi.org/10.1016/0022-5096(95)00031-D.
[51] H.J. Qu, K.H. Yano, P.V. Patki, M.J. Swenson, J.P. Wharry, Understanding plasticity in irradiated alloys through TEM in situ compression pillar tests, J. Mater. Res. 35 (8) (2020) 1037–1050, https://doi.org/10.1557/jmr.2019.295.
[52] X. Xiao, D. Terentyev, L. Yu, Model for the spherical indentation stress-strain relationships of ion-irradiated materials, J. Mech. Phys. Solids 132 (103) (2019) 694, https://doi.org/10.1016/j.jmps.2019.103694.
[53] C.D. Hardie, S.G. Roberts, A.J. Bushby, Understanding the effects of ion irradiation using nanoindentation techniques, J. Nucl. Mater. 462 (2015) 391–401, https://doi.org/10.1016/j.jnucmat.2014.11.066.
[54] Y. Zayachuk, D. Armstrong, K. Bystrov, S. Van Boxel, T. Morgan, S. Roberts, Nanoindentation study of the combined effects of crystallography, heat treatment and exposure to high-flux deuterium plasma in tungsten, J. Nucl. Mater. 486 (2017) 183–190, https://doi.org/10.1016/j.jnucmat.2017.01.026.
[55] C.D. Hardie, S.G. Roberts, Nanoindentation of model Fe–Cr alloys with self-ion irradiation, J. Nucl. Mater. 433 (1–3) (2013) 174–179, https://doi.org/10.1016/j.jnucmat.2012.09.003.

[56] B.N. Singh, A. Horsewell, P. Toft, Effects of neutron irradiation on microstructure and mechanical properties of pure iron, J. Nucl. Mater. 271–272 (1999) 97–101, https://doi.org/10.1016/S0022-3115(98)00767-3.

[57] B.C. Larson, W. Yang, G.E. Ice, J.D. Budai, J.Z. Tischler, Three-dimensional X-ray structural microscopy with submicrometre resolution, Nature 415 (6874) (2002) 887–890, https://doi.org/10.1038/415887a.

[58] W. Liu, G.E. Ice, B.C. Larson, W. Yang, J.Z. Tischler, J.D. Budai, The three-dimensional X-ray crystal microscope: a new tool for materials characterization, Metall. Trans. A, Phys. Metall. Mater. Sci. 35 (7) (2004) 1963–1967, https://doi.org/10.1007/s11661-004-0145-1.

[59] S. Das, W. Liu, R. Xu, F. Hofmann, Helium-implantation-induced lattice strains and defects in tungsten probed by X-ray micro-diffraction, Mater. Des. 160 (2018) 1226–1237, https://doi.org/10.1016/j.matdes.2018.11.001.

[60] J.S. Chung, G.E. Ice, Automated indexing for texture and strain measurement with broad-bandpass x-ray microbeams, J. Appl. Phys. 86 (9) (1999) 5249–5255, https://doi.org/10.1063/1.371507.

[61] J.Z. Tischler, LaueGo, Argonne National Laboratory, 2020.